May, 1979

Interaction of a compressional impulse with a slot normal to the surface of an elastic half space

A. Ilan
Leonard J. Bond
M. Spivack

Geophys. J. R. astr. Soc. (1979) **57**, 463–477

Interaction of a compressional impulse with a slot normal to the surface of an elastic half space

A. Ilan*, L. J. Bond and M. Spivack *Department of Physics, The City University, Northampton Square, London EC1V 0HB*

Received 1978 October 31; in original form 1978 July 19

Summary. An improved finite difference scheme is applied to simulate wave propagation in the vicinity of a slot normal to the surface of an elastic half space. It provides visualization of the scattered wave pattern at a sequence of time steps, and also the components of displacement as functions of time at a series of observation points.

After being hit by a normally incident plane *P* pulse, the slot oscillates with two main cycles and two shear-compressional pairs of diffracted waves, and also Rayleigh pulses, are scattered from it. The resulting wavefronts are parallel to the vertical surfaces of the slot and curve in semicircular arcs around the bottom of the slot.

Experimental tests of the theory were performed, using 0.5–6 MHz ultrasonic pulses on duralumin cylinders with surface-breaking slots ranging from 0.5–2 mm in width and from 2–6 mm in depth. The numerical results were confirmed by these experiments.

Introduction

The study of the pattern of elastic waves scattered by irregularities in a stress-free surface is important for seismology as well as for ultrasonic non-destructive testing.

Expressions for first-order scattering by small variations in the surface topography were first obtained by Gilbert & Knopoff (1960) and developed since by many investigators. The various methods used are summarized in a survey paper by Hudson (1977). They apply mainly to scatterers with slopes at small angles to the surface, and with dimensions which are not large in comparison with the initial wavelength. These methods are applicable to regions remote from the scatterer.

Recently several papers have calculated the displacements on the surface of the irregularity, mainly with steep slopes and prominent topographic features. Boore (1972b, 1973); Trifunac (1973); Wong & Trifunac (1974); Wong & Jennings (1975) deal with an *SH* initial disturbance, while Bouchon (1973) includes also *P* and *SV* incident waves. All found that the incident wave is considerably affected by the irregularity and that the effect

* Formerly with the Department of Geophysics and Planetary Sciences, Tel-Aviv University, Israel.

depends on the frequency and the angle of incidence of the initial wave. In geophysics, regions of amplification occur at the summits of mountains whereas attenuation is found at the bottom of depressions.

In the present paper, a finite difference method is applied to study the motion of a slot normal to the surface of an elastic half space, as well as the scattering pattern due to a normally incident *P* pulse.

Model assumptions

The medium is assumed to be perfectly elastic, isotropic and homogeneous with compressional and shear velocities α and β respectively. The geometry is a half space with a slot normal to its surface. Let the y axis be along the length of the slot, and x be parallel to the free surface, and let z point vertically upwards. Let D, l be the depth and width of the slot respectively. A plane compressional pulse is incident at an angle e to the half-space surface. The problem is thus two dimensional, and is as shown in Fig. 1.

Several sizes of the slot are considered where the ratio of the initial pulse width L to the depth of the slot, D, is such that $5 \geqslant L/D \geqslant 1$. Also L/l varies between 2 and 5.

INITIAL CONDITIONS

Let us assume that the sources of disturbance cause a compressional impulsive plane wave. The initial function describing such a waveform has been obtained by the following procedure adapted from Boore (1972a).

The input motion is required to fulfil the equations of motion in an infinite space. Let ψ be the scalar potential and U, W be the horizontal and vertical components of displacement respectively. Thus

$$U = -\frac{\partial \psi}{\partial x}; \qquad W = -\frac{\partial \psi}{\partial z}, \tag{1}$$

while the equation of wave motion is

$$\frac{1}{\alpha^2}\frac{\partial^2 \psi}{\partial t^2} = \frac{\partial^2 \psi}{\partial z^2} + \frac{\partial^2 \psi}{\partial x^2}. \tag{2}$$

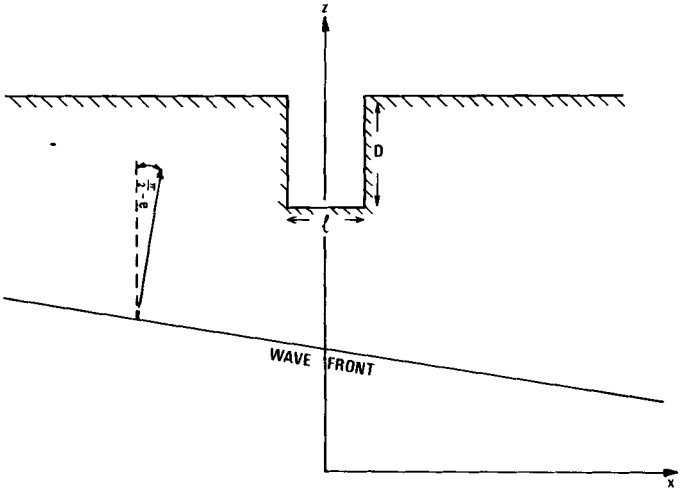

Figure 1. Cross-section of the model.

The plane wave approaching the surface at an angle e can be represented as follows:

$\psi = g[t - [x \cos(e) + z \sin(e)]/\alpha]$

where $g(\xi)$, for $\xi = t - (x \cos(e) + z \sin(e))/\alpha$, is an arbitrary waveform.

Using the finite difference method, the accuracy of the numerical results improves as the initial function is made smoother, as Ilan & Loewenthal (1976) and others have shown. To achieve this, the initial function was obtained by first integrating the Dirac delta function five times.

$$G_1 = \int_0^{\xi} \delta(\eta)\, d\eta = H(\xi),$$

where H is the Heaviside step function,

$$G_2 = \int_0^{\xi} G_1(\eta)\, d\eta$$

.

.

.

$$G_5 = \xi^4/4!\, H(\xi). \tag{3}$$

Then five consecutive central finite differences of G_5 were taken over an arbitrary interval Δ. The function has been normalized to be unity at $\xi = 0$. This gives a smoothed δ function,

$$\langle\delta(\xi)\rangle = [G_5(\xi + 5\Delta) - 5G_5(\xi + 3\Delta) + 10G_5(\xi + \Delta) - 10G_5(\xi - \Delta) + 5G_5(\xi - 3\Delta) - G_5(\xi - 5\Delta)]/(230\Delta^4) \tag{4}$$

and

$U = \cos(e)\langle\delta(\xi)\rangle; \qquad W = \sin(e)\langle\delta(\xi)\rangle.$

The initial displacement for the case of $e = \pi/2$ is shown in Fig. 2. The width L of the initial pulse is defined to be $L = 10\,\Delta$. In the first stage, normally incident waves were assumed.

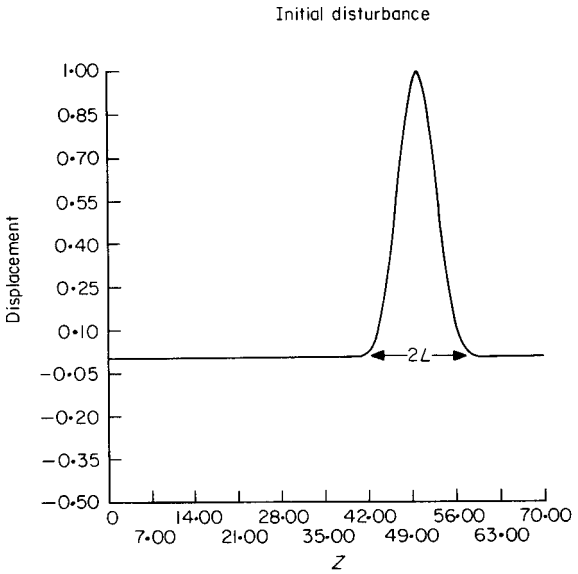

Figure 2. The displacement due to the initial pulse.

Finite difference formulation

A square grid with increment h is superimposed on the x, z plane. Thus $x = (j-1)h; j = 1, M$, and $z = (k-1)h; k = 1, N$, and h is also defined as the unit of length. The time increment Δt is chosen in such a way that the von-Neumann criterion of stability is fulfilled in the form derived by Alterman & Loewenthal (1970),

$$\Delta t \leqslant h/\sqrt{\alpha^2+\beta^2}. \tag{5}$$

In the following calculations the initial wave pulse was spread over 18 grid units. This guarantees that aliasing errors and numerical dispersion (see Boore 1972a) do not affect the results.

Let $U^p_{j,k}$, $W^p_{j,k}$ be the components of displacement at the grid point (j, k) at time level p. An explicit formula for calculating the displacements of inner points was obtained by replacing the derivatives in the equation of motion with central finite differences. This formula was given by Alterman & Loewenthal (1970) and many others and will not be repeated here. On the stress-free surface the new composed approximation by Ilan & Loewenthal (1976) was used. This approximates the boundary conditions to the second order of accuracy and does not need the aid of fictitious lines (as do previous schemes). The formulae for the components of displacement on the horizontal stress-free surface are:

$$\begin{aligned}
U^{p+1}_{j,k} &= -U^{p-1}_{j,k} + 2\left[1 - 2\epsilon\beta^2(2-\beta^2/\alpha^2)\right]U^p_{j,k} + 2\epsilon\beta^2 U_{j,k-1} \\
&\quad + \epsilon\beta^2(3-2\beta^2/\alpha^2)\,(U^p_{j+1,k} + U^p_{j-1,k}) - \epsilon\beta^2(W^p_{j+1,k} - W^p_{j-1,k}) \\
W^{p+1}_{j,k} &= -W^{p-1}_{j,k} + 2\left[1 - \epsilon(\alpha^2+\beta^2)\right]W^p_{j,k} + 2\epsilon\alpha^2 W^p_{j,k-1} + \epsilon\beta^2(W^p_{j+1,k} + W^p_{j-1,k}) \\
&\quad + 0.5\,\epsilon(3\beta^2-\alpha^2)\,(U^p_{j+1,k} - U^p_{j-1,k}) - 0.5\,\epsilon(\alpha^2-\beta^2)\,(U^p_{j+1,k-1} - U^p_{j-1,k-1})
\end{aligned} \tag{6}$$

where $\epsilon = \Delta t^2/h^2$.

On the vertical stress-free surface, equations (6) can be applied after transforming them in the following manner:

$$U \to W; \quad W \to U; \quad \partial x \to \partial z; \quad \partial z \to \partial x.$$

Here ∂x indicates differentiation with respect to x.

The displacements at the 90° corner were calculated by the method of Alterman & Loewenthal (1970) and at the 270° corner by that of Ilan, Unger & Alterman (1975). This scheme was carefully examined by Ilan & Loewenthal (1976) and Ilan (1978) and was found to be stable and to give accurate results in half-planes and quarter-planes for a wide range of elastic parameters.

For a normally incident wave the problem is symmetric with axis of symmetry along $x = x_0$, where x_0 passes through the centre of the bottom of the slot. It is sufficient to calculate the scattered field on the right of the axis, and to impose the following conditions at $x = x_0$:

$$U = 0; \quad \frac{\partial W}{\partial x} = 0. \tag{7}$$

Conditions (7) were assumed also on the right boundary of the grid while on the lowest horizontal grid line boundary, the components of displacement were assumed to be zero. This delays artificial reflections from the grid boundaries up to the time when the first diffracted pulse arrived at the edges of the grid. Usually a grid of 60 × 60 points was used.

The values at the first and second time steps are known by equations (3), (4). The explicit finite difference scheme provides a process to compute the displacements at successive time levels. No presuppositions are made about the solution and the various phases are computed simultaneously.

Results

In order to analyse the results the data were represented in two different ways. In the first, positions of all the grid particles were plotted at certain intervals of time in a manner adapted from Munasinghe (1973). In the second representation, components of displacement at a series of chosen observation points were stored and eventually plotted as functions of time. This enables us to consider the excited area at consecutive time steps and to study the features of the scattered wavefronts and the direction of displacements. Measuring the positions of a certain wavefront at different time levels enables us to determine its velocity of propagation. Thus a better insight is obtained into the interaction between a compressional pulse and a vertically cut slot.

SLOT DISTORTION

The shape of the slot at consecutive time steps after it has been hit by a normally incident compressional pulse is shown in Fig. 3. The slot depth D is a third of the pulse length L and the ratio of the slot width l to its depth is 2/3. The displacements in Fig. 3 are amplified by a factor of 2 in order to emphasize the slot distortion.

After being hit by the initial pulse, the slot surface begins to bow in and out, to stretch and compress in quite a complicated manner. Two main cycles of vibration can be distinguished apparently due to the initial and reflected waves. The vibration of the slot continues afterwards but attenuates rapidly. It appears that after the initial pulse has hit the upper corners two surface waves are created and propagate along the flanks with

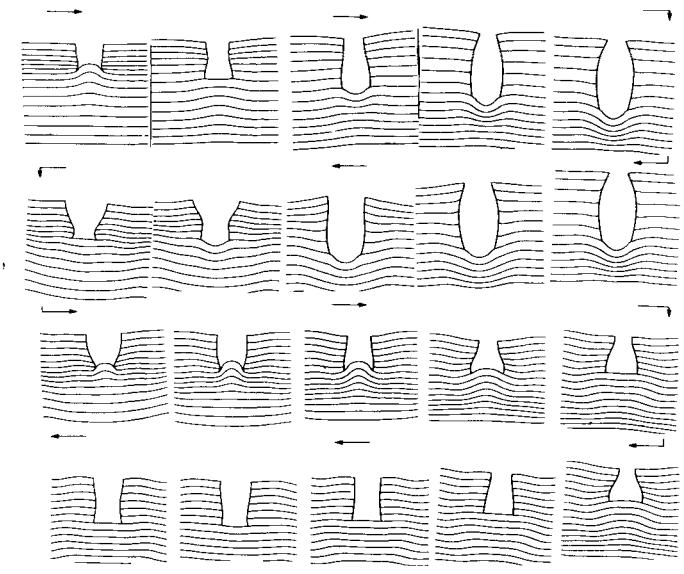

Figure 3. The slot shape due to a vertically incident P pulse at consecutive times, as indicated by the arrows. $D/L = 1/3, l/D = 2/3$. The displacements are amplified by a factor of 2.

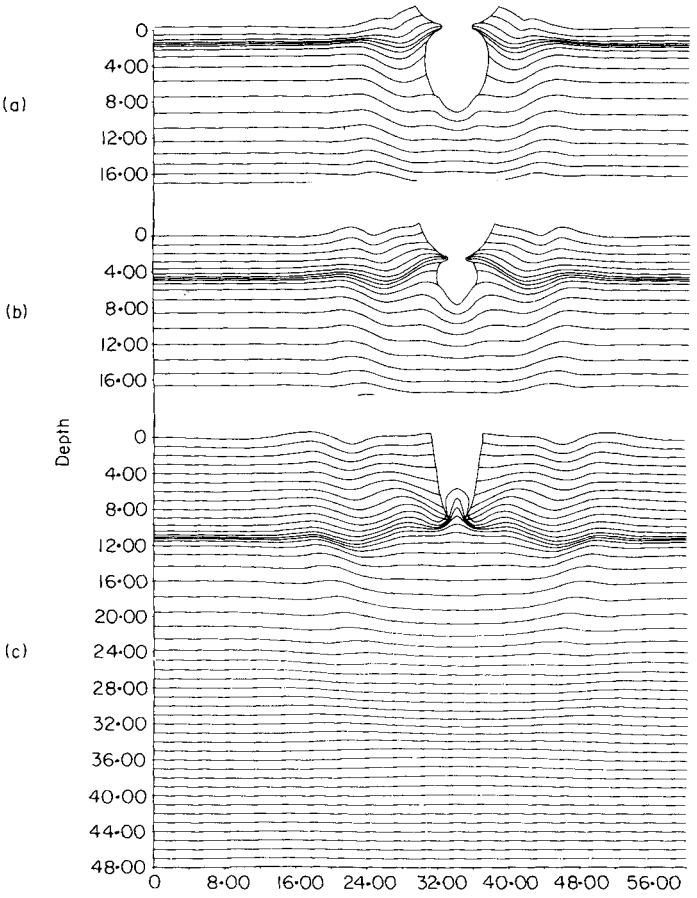

Figure 4. Cross-section of the model at three time levels, $t\alpha/h = 28, 31, 38$. The displacements are amplified four times. $D/L = 1/2; l/D = 4/9$.

Rayleigh wave velocity. They superpose at the bottom and proceed upwards as is demonstrated in Fig. 4. The vertical component of displacement is attenuated at the bottom and along the flanks of the slot. Attenuation of 20 per cent occurs at the lower corner. On the other hand, the off-axis points of the slot surface acquire horizontal displacements. The maximum amplitude occurs at the upper corners and was found to be 0.65 of the amplitude of the initial pulse for the case of $D/L = 1/3, l/d = 2/3$.

These results are generally in agreement with Bouchon (1973).

THE SCATTERED FIELD

For the case of 90° incidence the main energy is obviously reflected normally. In addition, a diffraction pattern is created as follows: after arriving at the bottom of the slot the initial pulse excites a shear and a compressional pulse which propagate in an almost semicircular wavefront around the mid-point of the bottom of the slot. After arriving at the surface and being normally reflected, the main disturbance also creates a Rayleigh and a compressional wave propagating in wavefronts parallel to the vertical surfaces. The second cycle of the slot distortion causes a similar pair of diffracted waves with wavefronts parallel to the first

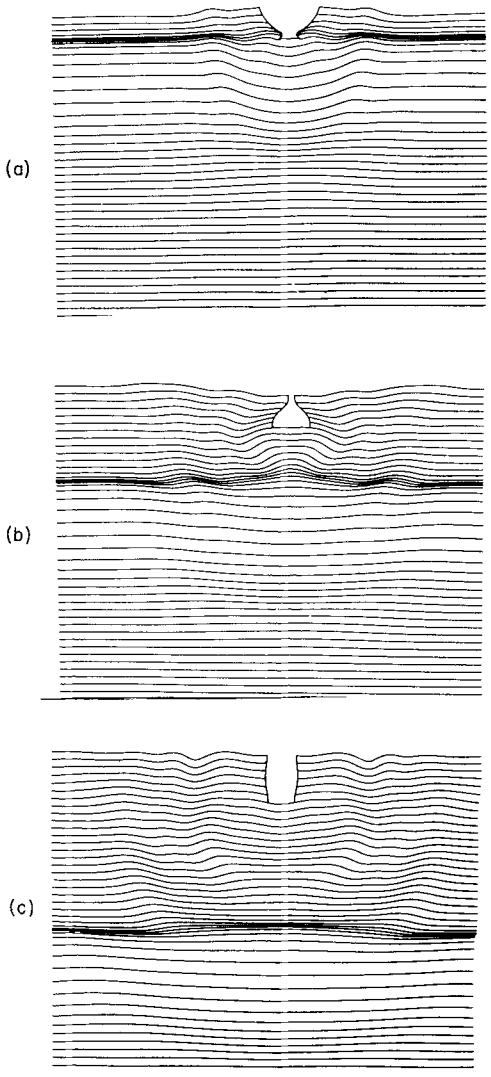

Figure 5. Cross-section of the model at three time levels, $t\alpha/h = 30, 39, 50$, due to a vertically incident P pulse. $D/L = 1/3, l/D = 2/3$.

diffraction but with reduced amplitude. The position of the particles in the vicinity of the slot at three time levels is shown in Fig. 5.

In Fig. 5(a) the main pulse has been reflected and the first diffraction can be seen. At the second time level (Fig. 5(b)) the first diffracted wave has propagated forwards and a second wavefront has just been created. In the third stage, the slot has almost calmed down and the main pattern of scattered waves can be seen. Plotting the particle positions by horizontal lines emphasizes the vertical but not the horizontal displacements. In order to complete the wave pattern, the particle positions were plotted also by vertical lines as demonstrated in Fig. 6. In this case the slot depth D is half the pulse width and $l/D = 4/9$. The displacements were exaggerated four times in Fig. 6(a), and eight times in Fig. 6(b). The scattering pattern is clarified by considering time series at certain observation points. In Fig. 7 these points

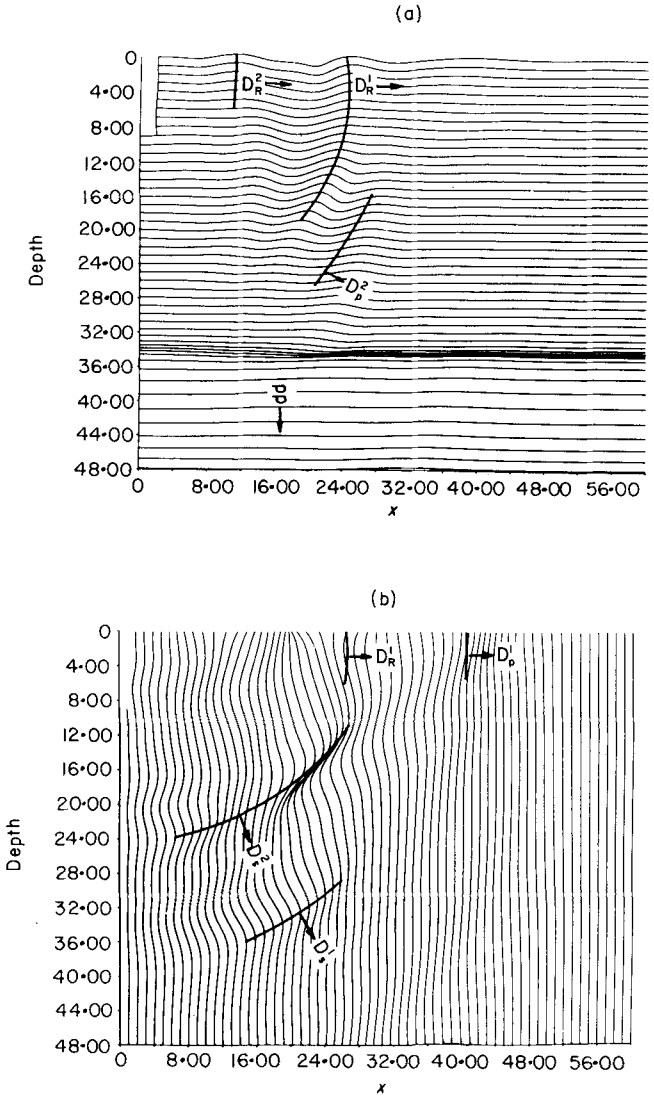

Figure 6. Section of a half plane with a slot to the right of the axis of symmetry at time level $t\alpha/h = 60$. The displacements are amplified by the factors; (a) 4, (b) 8. D_p^i, D_s^i; $i = 1, 2$ are the diffracted compressional, shear and Rayleigh pulses respectively. $D/L = 1/2, l/D = 4/9$.

were situated on the free surface at various horizontal distances from the slot. The initial pulse arrives simultaneously at all the observation points and has only a vertical component. The seismograms of the vertical component show also the two Rayleigh diffracted waves and those of the horizontal component show also the compressional diffracted pulses. The time interval between two successive diffracted waves increases as the slot is made deeper or wider. In Fig. 8 the observation points are situated $21\,h$ from the slot at various depths. Here the diffracted pulses arrive simultaneously at receivers situated at depths less than or equal to that of the slot. When the receiver is located deeper than the slot the arrival time increases due to the increasing distance from the scatterer. In Fig. 9 the observation points are located at a constant depth of one pulse length at various horizontal positions.

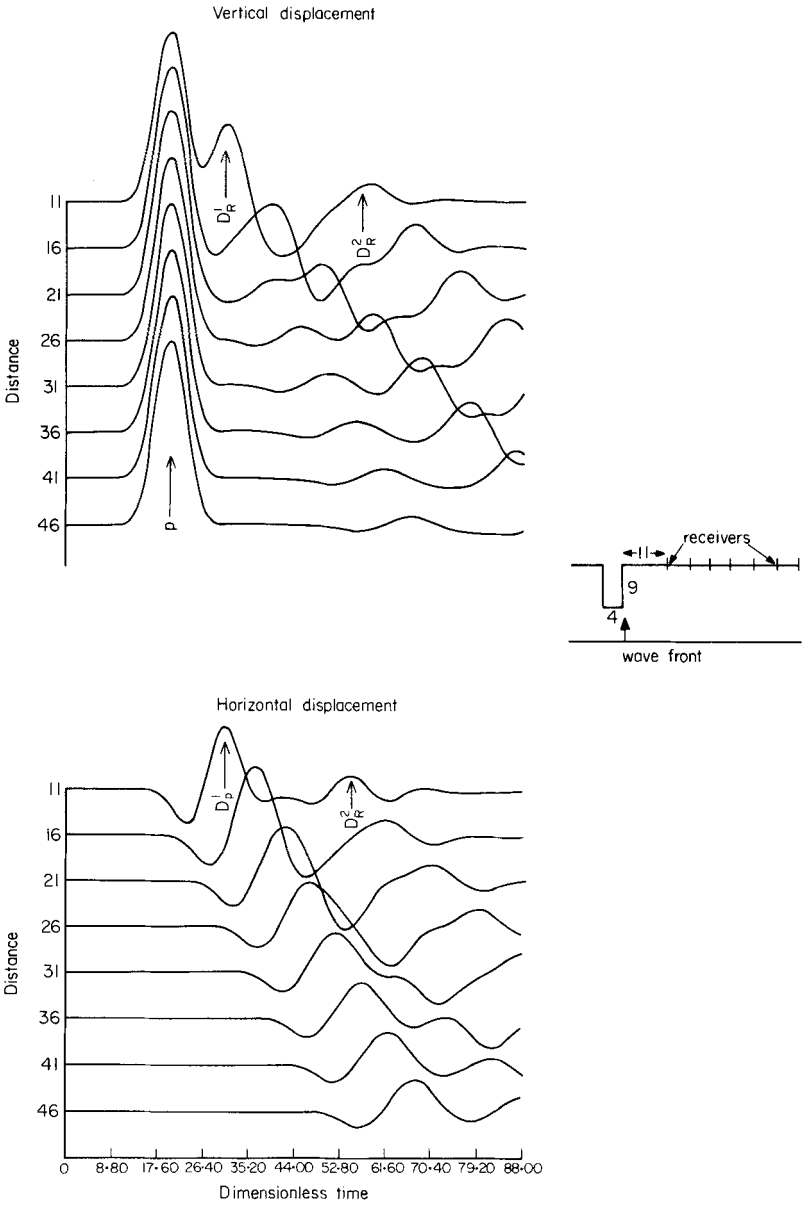

Figure 7. Displacements on the surface of an irregular half space as functions of time in units of h/α at various distances from the slot. A schematic model is on the right. $D/l = 1/2$, $l/D = 4/9$. The other details are as in Fig. 6.

The first arrival is the compressional pulse diffracted from the bottom of the slot. The next pulse is the main compressional reflection arriving simultaneously at all the observation points. The two shear pulses diffracted from the bottom of the slot can be seen in the seismograms of the horizontal component.

The results shown in Fig. 10 were obtained with receivers situated on the central axis at various distances R from the bottom of the slot. Fig. 10(a) shows the amplitude of the

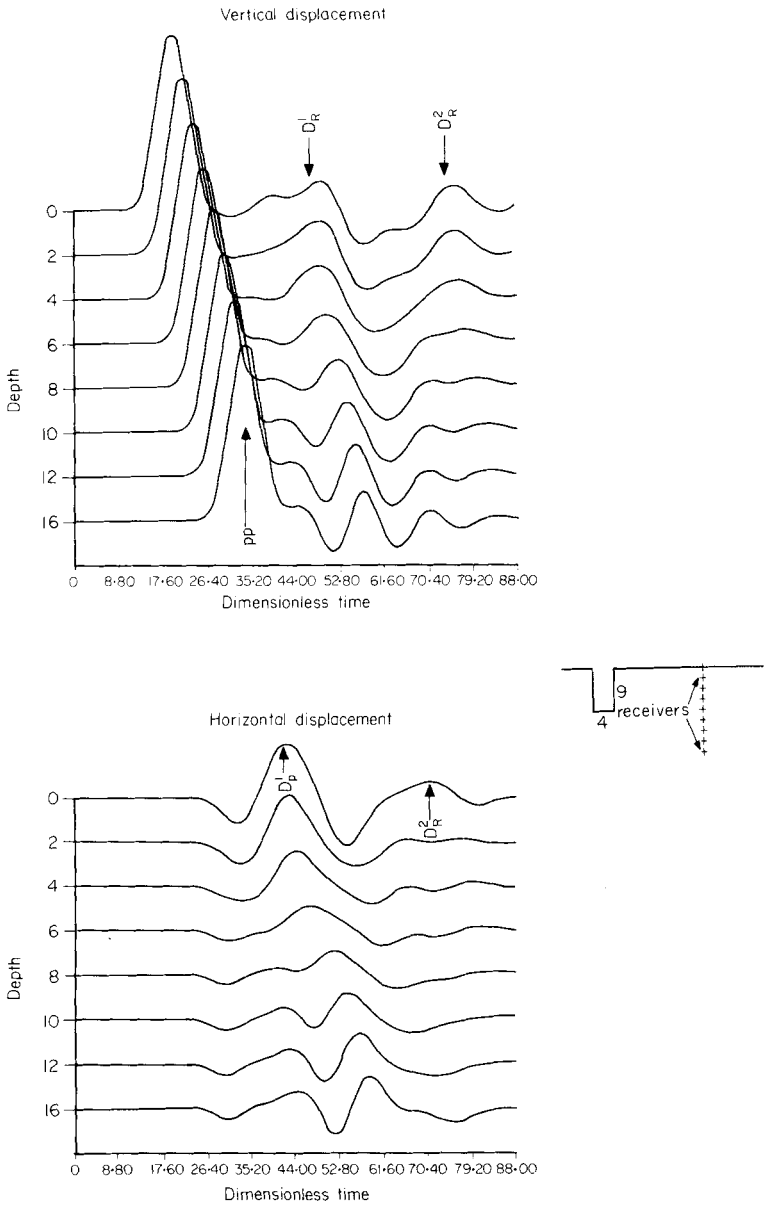

Figure 8. Displacements against time at a distance $21h$ from the centre of the slot at various depths. The other details are as in Fig. 6.

first compressional diffracted pulse, and Fig. 10(b) the amplitude of the reflected pulse as functions of R/L, for slots with constant depth and different widths. The amplitude of the first diffracted pulse, D_p^1, increases considerably as l/L is made larger, as shown in Fig. 10(a). It decreases with the distance from the scatterer as is expected for radially propagated waves. Similar results were obtained for several depths of slots. The depth of the slot was found to have only secondary influence on the amplitude of the diffracted pulses. For very shallow slots D_p^1 and PP are superimposed but they become separated for $D/L \geqslant 0.22$.

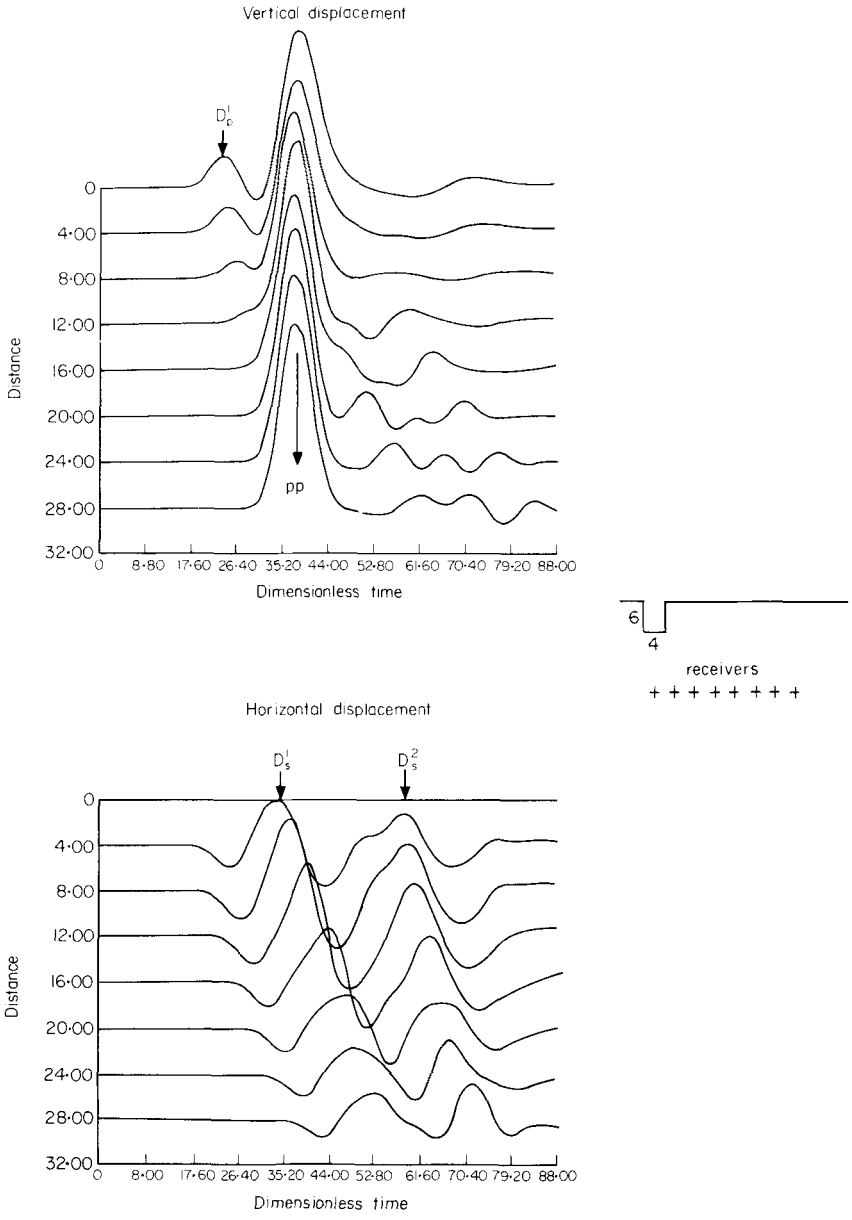

Figure 9. Displacements against time at a depth of $18h$ equal to the pulse length L at various horizontal distances. The scale of the horizontal displacements is twice that of the vertical ones. The other details are as in Fig. 6.

The amplitude of the first shear diffracted pulse, D_s^1, is zero on axis and varies with the angle from the axis, reaching a maximum value for an angle between 35–45°, as shown in Fig. 9. The maximum amplitude of D_s^1 increases directly with l/L and is approximately half the maximum amplitude of D_p^1.

The normally reflected pulse travels around the vertical boundaries of the slot, but its amplitude is reduced due to mode conversion. This reduction takes place even for shallow

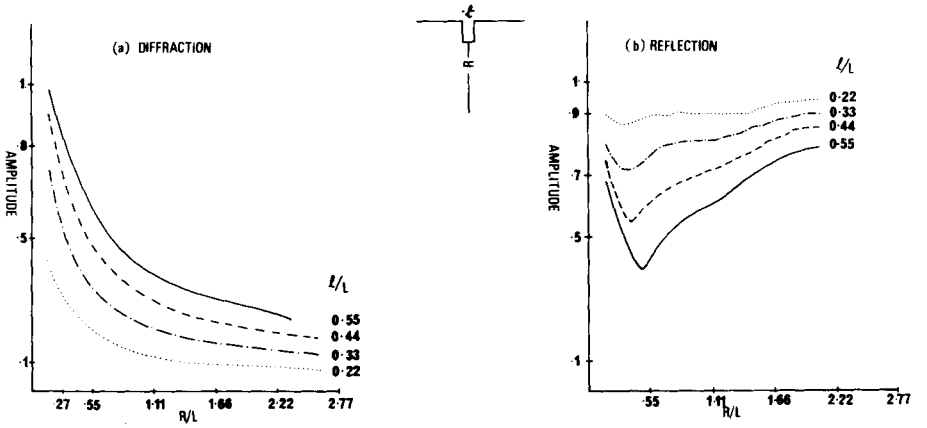

Figure 10. Amplitudes of diffracted and reflected pulses as functions of the distance from the bottom of the slot. The distance is in units of the pulse length L. $D/L = 1/3$ and l/D varied as indicated. The observation points are situated along the z axis.

slots where $D/L = 0.11$. A shadow zone can be seen under the slot; this zone becomes wider and deeper as l/L is made larger, as shown in Fig. 10(b). Here $D/L = 1/3$ and $0.22 \leqslant l/L \leqslant 0.55$. The amplitude of the reflected pulse depends mainly on the width of the slot, and it decreases as l/L increases.

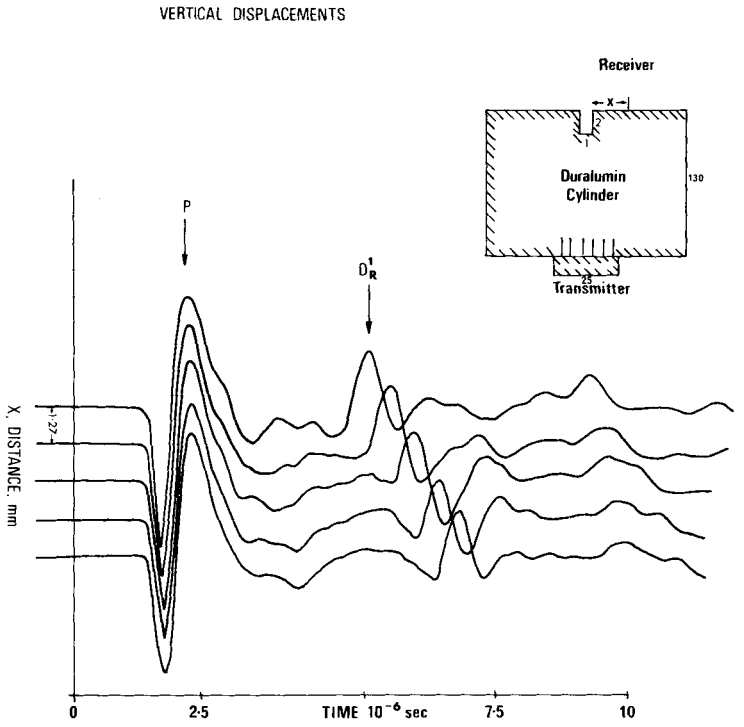

Figure 11. Ultrasonic pulse in a cylinder containing a surface-breaking slot. On the right is a schematic diagram of the experiment where the model dimensions are indicated in mm, and the wavelength is 3 mm.

Comparison with experimental results

Experiments were carried out using ultrasonic waves in a duralumin cylinder. The compressional wave velocity α in duralumin is 5327 m/s and $\beta/\alpha = 0.48$. The cylinder was 10 cm in diameter and 13 cm in height with a slot cut along the diameter normally to the surface. In the first experiment, shown in Fig. 10, the slot had 2 mm depth and 1 mm width. A cylindrical compressional wave transducer, 25 mm in diameter, was carefully bonded to the opposite surface as indicated. It emitted a single-cycle pulse centred on 2.37 MHz which corresponds approximately to a 3 mm wavelength.

The receiver was a thin (about 0.2 mm) broadband probe as designed by Harnik (1977). It was oriented perpendicularly to the surface and parallel to the slot at various distances (increasing by steps of 1.27 mm) from the slot. The vertical displacements plotted against time are shown in Fig. 11. The first pulse, arriving after the incident *P* pulse, propagates from the slot with Rayleigh wave velocity. This is similar to the numerical results depicted in Fig. 7. The identification of Rayleigh waves was confirmed by replacing Harnik's probe by another receiver which is sensitive to Rayleigh waves only.

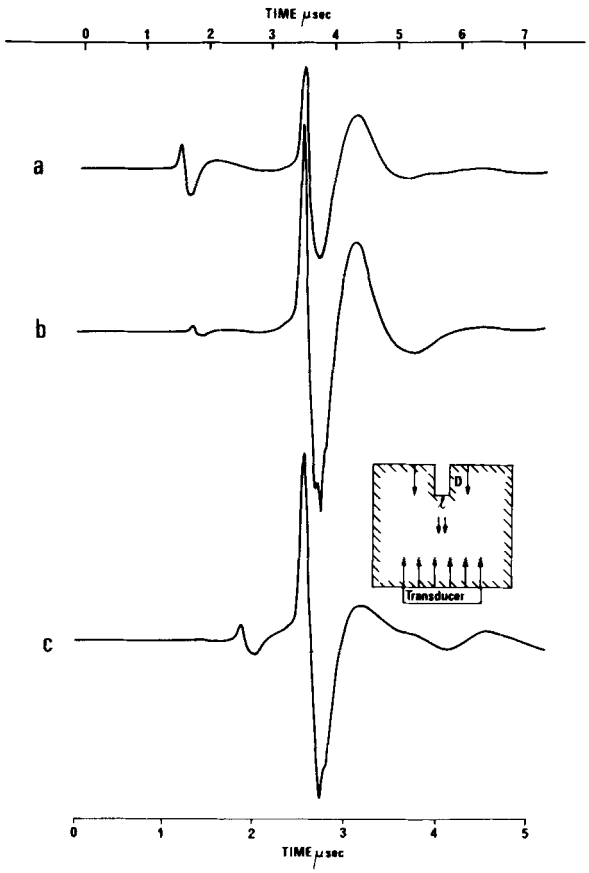

Fig. 12. Vertical displacements as functions of time due to ultrasonic pulses. On the right is a schematic diagram of the experimental disposition. The transducer operates as both transmitter and receiver and emits pulses centred on: (a) and (b) 1.5 MHz, (c) 2.37 MHz. The dimensions in mm of the slots are: (a) $D = 6, l = 2$, (b) $D = 5, l = 0.5$, (c) $D = 2, l = 1$.

In the second experiment the transducer, which is situated on the surface opposite the slot, operates also as a receiver. The time series of the displacements associated with slots of three different sizes were obtained and are shown in Fig. 12. Here, as in the numerical results shown in Fig. 9, the precursor to *PP* is a *P* pulse diffracted from the bottom of the slot. The depths of the different slots were 5, 2, 6 mm and their widths were 0.5, 1, 2 mm respectively. The ratios between the amplitudes of the diffracted and the reflected pulses were 0.03, 0.08, 0.21 respectively. This ratio increases as the slot is made wider, which agrees with the computed results in Fig. 10. Direct comparison is not possible here because the experimental measurements were made in a region much further from the scatterer.

The ratio between the amplitude of the diffracted and the reflected pulses indicates the slot width. The slot depth can be accurately calculated using the difference between the arrival times of the two pulses. In comparing the numerical with the experimental results one has to bear in mind that in the experimental, but not in the numerical, case the wavefront and the medium are of finite dimensions. Therefore edge waves from the boundary of the transducer and their various reflections are included in the experimental time series.

In the laboratory, the probe is located on the surface and detects one component of displacement only, whereas using the finite difference method any observation point can be chosen and both components of displacement may be calculated simultaneously. Thus the numerical results provide a broader understanding of the scattering phenomena while the experimental results confirm some of the conclusions and do not contradict any of them.

Conclusions

The improved finite-difference method of Ilan & Loewenthal (1976) was used to obtain the scattered field of a compressional impulse in the vicinity of a surface irregularity.

First a simple case was considered; that of a compressional pulse normally incident at a slot cut vertically in the surface. Analysis of the numerical results shows that, after being hit by the initial pulse, the slot begins to oscillate with two main cycles of vibration. Every surface point becomes a source of a compressional and a shear diffracted wave, as is predicted by Huyghens' theory. The contributions of the various source points combine to form scattered wavefronts which are parallel to the vertical surfaces of the slot and semi-circular around the bottom of the slot. The second cycle of vibration excites a second wavefront with reduced amplitude.

The amplitude of the scattered pulses depends mainly on the ratio of the width of the slot to the initial pulse width, l/L. The amplitude of the diffracted pulses increases as l/L increases. The amplitude of the reflected pulse is reduced in a shadow zone under the slot, which becomes wider and deeper as l/L increases.

Research is continuing on the more general scattering problems which arise when non-normally incident waves are applied or when *SH*, *SV* and Rayleigh waves are incident.

Acknowledgments

We wish to thank Professor A. F. Brown for reading the manuscript and for his helpful comments. We wish also to thank Mr J. P. Weight for his help in carrying out the experiments.

The authors have received support from, respectively, the NERC, the MOD and the SRC in collaboration with the British Gas Corporation under the CASE scheme.

References

Alterman, Z. & Loewenthal, D., 1970. Seismic waves in a quarter and three-quarter plane, *Geophys. J. R. astr. Soc.*, **20**, 101–126.

Boore, D. M., 1972a. Finite difference methods for seismic wave propagation in heterogeneous materials, chapter 5 in *Methods in Computational Physics*, **11**, 1–37, Academic Press, New York.

Boore, D. M., 1972b. A note on the effect of simple topography on seismic *SH* waves, *Bull. seism. Soc. Am.*, **62**, 275–284.

Boore, D. M., 1973. The effect of simple topography on seismic waves. Implications for accelerations recorded at Pacoima Dam, San Fernando Valley, California, *Bull. seism. Soc. Am.*, **63**, 1603–1609.

Bouchon, M., 1973. Effect of topography on surface motion, *Bull. seism. Soc. Am.*, **63**, 615–632.

Gilbert, J. F. & Knopoff, L., 1969. Seismic scattering from topographic irregularities, *J. geophys. Res.*, **65**, 3437–3444.

Harnik, E., 1977. A broadband probe for studies of acoustic surface waves, *J. Phys. E, Sci. Inst.*, **10**, 1217–1218.

Hudson, J. A., 1977. Scattered waves in the coda of *P*, *J. Geophys.*, **43**, 359–374.

Ilan, A., 1978. Stability of finite difference schemes for the problem of elastic wave propagation in a quarter plane, *J. Comp. Phys.*, **29**, 389–403, the Z. Alterman Memorial Volume.

Ilan, A. & Loewenthal, D., 1976. Instability of finite difference schemes due to boundary conditions in elastic media, *Geophys. Prosp.*, **24**, 431–453.

Ilan, A., Ungar, A. & Alterman, Z. S., 1975. An improved representation of boundary conditions in finite difference schemes for seismological problems, *Geophys. J. R. astr. Soc.*, **43**, 727–742.

Munasinghe, M., 1973. Numerical solutions for acoustic Rayleigh waves scattering in discontinuous media, *PhD thesis*, McGill University, Canada.

Trifunac, M. D., 1973. Scattering of plane *SH* waves by a semi-cylindrical canyon, *Int. J. Earthquake Eng. Struct. Dyn.*, **1**, 267–281.

Wong, H. L. & Jennings, P. C., 1975. Effects of canyon topography on strong ground motion, *Bull. seism. Soc. Am.*, **65**, 1239–1257.

Wong, H. L. & Trifunac, M. D., 1974. Scattering of plane *SH* waves by semi-elliptical canyon, *Int. J. Earthquake Eng. Struct. Dyn.*, **3**, 157–169.